研 究 速 報

Mesoscopic Analysis of Ductile Fracture with Void Linking by Using Natural Element Method

Yutaka TOI* and Sung-Soo KANG*

1. Introduction

The two-dimensional mesoscopic method of analysis using Natural Element Method[1] (abbreviated as NEM) previously proposed by the authors[2-5] is applied to the fracture analysis of ductile solids containing microvoids. Plates containing irregularly distributed circular holes are studied as models of two-dimensional solids with microvoids. The validity of the proposed method is demonstrated by the mesoscale fracture analysis considering void linking.

2. Mesoscale Method of Analysis Using NEM

2.1 Theoretical basis of NEM

In NEM[1], a finite number of nodal points are distributed on an analyzed region. Shape functions are defined, using Voronoi polygons based on those nodal points, Delaunay triangles and their circumscribed circles.

When an arbitrary integration point $\mathbf{x}$ is located within the circumscribed circle of the Delaunay triangle (n_J, n_K, n_L), the nodal points n_J, n_K, n_L are defined as natural neighbors of the integration point $\mathbf{x}$. The second-order Voronoi polygon T_{IJ} is defined by eq. (1), in which T_{IJ} is a set of all points that have n_I as the nearest neighbor and n_J as the second nearest neighbor.

$$T_{IJ}=\left\{\mathbf{x}\in\mathbf{R}^2:d(\mathbf{x},\mathbf{x}_I)<d(\mathbf{x},\mathbf{x}_J)<d(\mathbf{x},\mathbf{x}_K)\forall K\neq I,J\right\} \quad (1)$$

Denoting the area of T_{XI} as $A_I(\mathbf{x})$, the shape function $\Phi_I(\mathbf{x})$ for the natural neighbour I is defined by the following equation:

$$\phi_I(\mathbf{x})=A_I(\mathbf{x})\,/\,A(\mathbf{x}) \quad (2)$$

where I is 1 to n and $A(\mathbf{x})=\sum_{J=1}^{n}A_J(\mathbf{x})$. n is the total number of natural neighbours of $\mathbf{x}$. The displacement functions are given as follows:

$$\mathbf{u}^h(\mathbf{x})=\sum_{I=1}^{n}\phi_I(\mathbf{x})\mathbf{u}_I \quad (3)$$

2.2 Microracking condition

A microcrack is assumed to occur along the edge of the Voronoi polygon, when the average of normal microstrains at the nearest integration points $\mathbf{x}_1$, $\mathbf{x}_3$, $\mathbf{x}_4$, $\mathbf{x}_5$ of each Voronoi edge reachs the critical value (see Fig. 1), that is,

$$\varepsilon_{ave}(=\sum\varepsilon_n\,/\,4)\geq\varepsilon_{cr} \quad (4)$$

where

$$\varepsilon_n=\frac{\varepsilon_x+\varepsilon_y}{2}+\frac{\varepsilon_x-\varepsilon_y}{2}\cos 2\theta+\frac{\gamma_{xy}}{2}\sin 2\theta \quad (5)$$

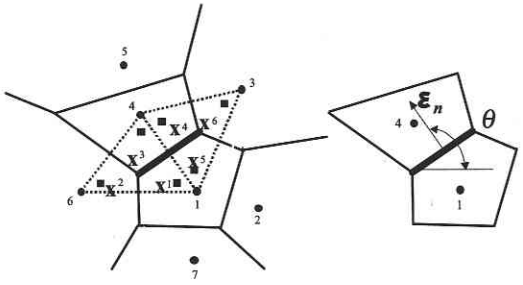

Fig. 1 Critical condition for microcracking

2.3 Modeling of microcracking

The Delaunay triangles lying on the microcracked Voronoi edge are removed from the searching of natural neighbour nodes of the integration point $\mathbf{x}$, when the shape function is calculated for an arbitrary integration point $\mathbf{x}$ (see Fig. 2). The effect of microcracking is considered in the calculation of shape functions by removing the mechanical coupling between nodes located at the

*Institute of Industrial Science, University of Tokyo

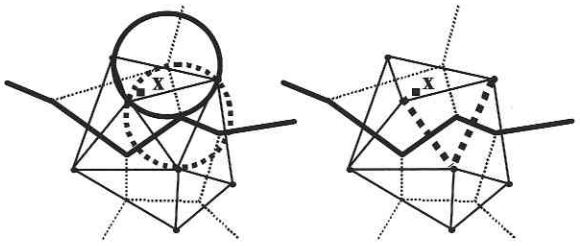

Fig. 2 Consideration of crack propagation

opposite sides of the microcrack. It is assumed that all edges of one Voronoi polygon are not microcracked in order to avoid the singularity of the stiffness matrix.

2.4 Incremental stiffness equation

The plane stress condition is assumed for the numerical examples in the following chapter. The elasto-plastic deformation is considered according to the incremental formulation. The tangential stress-strain matrix $\mathbf{D}_{ep}$ based on von Mises yield condition and associated normality flow rule with isotropic hardening is used at each integration point.

The incremental stiffness equation is given by the following equations:

$$\mathbf{K}\Delta\mathbf{u} = \Delta\mathbf{f} + \mathbf{f}_r \quad \cdots\cdots (6)$$

where

$$\mathbf{K} = \int_A \mathbf{B}^T\mathbf{D}_{ep}\mathbf{B}dA \quad \cdots\cdots (7)$$

$$\mathbf{f}_r = \int_A \mathbf{B}^T\mathbf{s}dA \quad \cdots\cdots (8)$$

$$\mathbf{s} = \begin{Bmatrix} \sigma_n \\ \sigma_s \\ \tau_{ns} \end{Bmatrix} \quad \cdots\cdots (9)$$

$$\mathbf{B}^T = \begin{bmatrix} \frac{\partial\phi}{\partial n} & 0 & \frac{\partial\phi}{\partial s} \\ 0 & \frac{\partial\phi}{\partial s} & \frac{\partial\phi}{\partial n} \end{bmatrix} \quad \cdots\cdots (10)$$

ϕ is the shape function for a node. $\mathbf{f}_r$ is the released force vector for the microcrack formed at the preceding incremental step in which the stress component σ_s in the parallel direction of the crack is assumed to be zero. It should be noted that the sign of the released force vector is opposite compared with the conventional finite element method cutting nodal connections, because the microcrack is formed on the Voronoi edge between adjacent nodes.

3. Numerical Examples

3.1 Void linking under uniaxial loading

The material analyzed is aluminum 3003 for which Young's modulus and Poisson's ratio are 70GPa and 0.33, respectively. The shape of the specimen and boundary conditions are shown in Fig. 3. 63 circular holes with a diameter 1.6mm are randomly distributed in the specimen. The area fraction of circular holes is 2%. The nodal distribution is shown in Fig. 4.

Fig. 5 shows the distribution of equivalent strain immediately before the microcracking near circular holes. It is seen that high

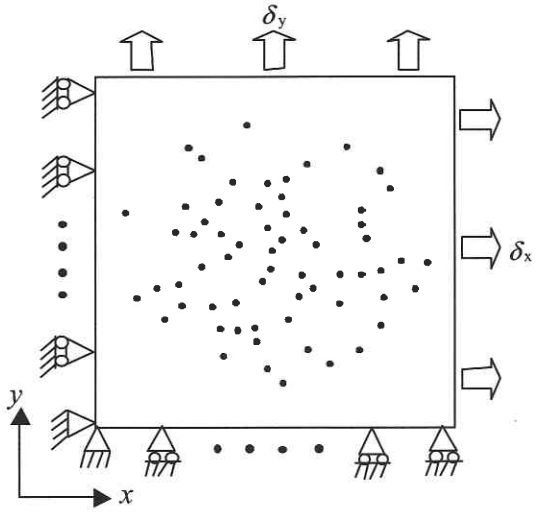

Fig. 3 Perforated sheet under uni/biaxial tension

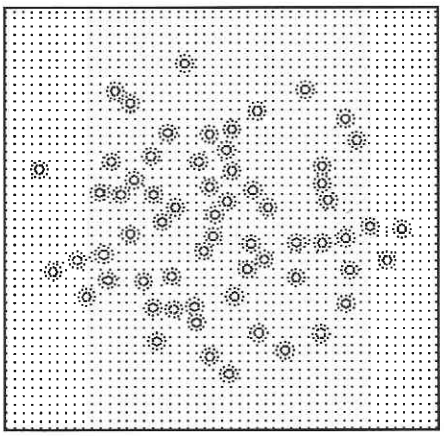

Fig. 4 Nodal arrangement

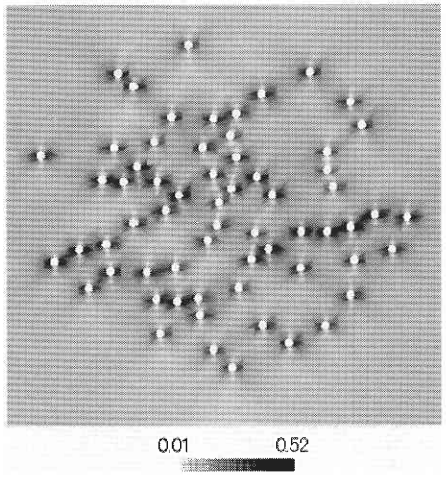

Fig. 5 Equivalent strain（uniaxial loading）

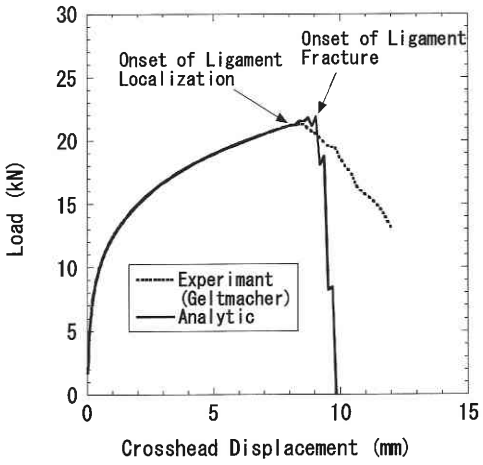

Fig. 6 Load-displacement curves（uniaxial loading）

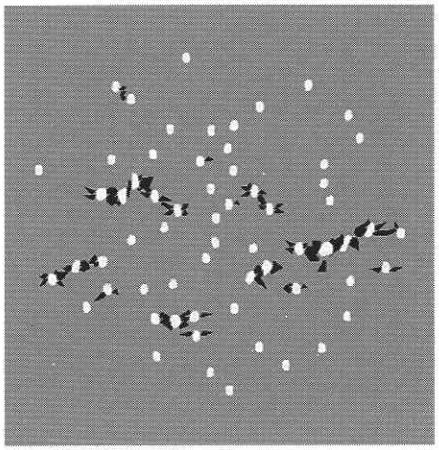

Fig. 7 Void linking（uniaxial loading, δ_y = 9.055 mm）

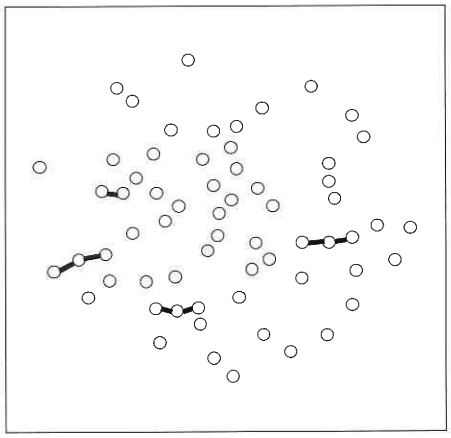

Fig. 8 Experimental void linking（uniaxial loading）

equivalent strain occurs between adjacent circular holes in the direction perpendicular to the tensile loading. Higher strain occurs between closer holes where microcracking easily takes place.

Fig. 6 shows calculated and experimental load-displacement (δ_y) curves. The ligament fracture occurs immediately after the localization of plastic deformation at the ligament strained in the loading direction. ε_{cr} in eq. (4) is determinded by the calculated strain at the ligament localization in the experiment[6]. The load-displacement curve after the peak load does not agree well with the experimental result, because the critical condition for microcracking is extremely simplified. The Delaunay triangles removed to disconnect mechanical coupling of adjacent nodes over the crack are shown in Fig. 7 with the deformation as an illustration of void linking, which agree well with the experimental cracking pattern[6] as shown in Fig. 8.

3.2 Void linking under biaxial loading

The shape and the boundary condition of the specimen is shown in Fig. 3.

Fig. 9 shows the distribution of equivalent strain immediately before the cracking around circular holes. High strain occurs on the ligaments in various directions in comparison with the case under uniaxial loading. The load-displacement curve is shown in Fig. 10 where the ligament fracture occurs immediately after the localization of plastic deformation on the ligament part. Fig. 11 shows the cracking and the deformation in a similar way to Fig. 7, which agree well with the experimental cracking pattern[6] shown in Fig. 12.

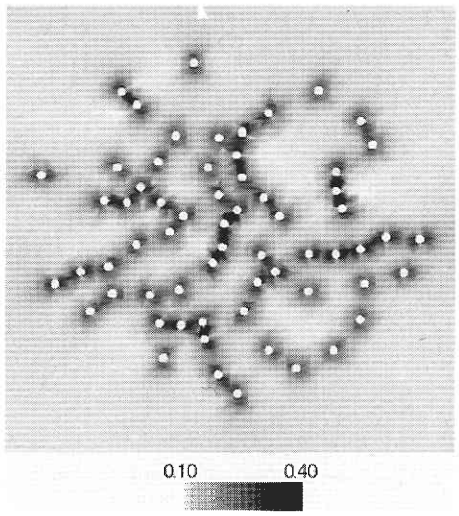

Fig. 9 Equivalent strain (biaxial loading)

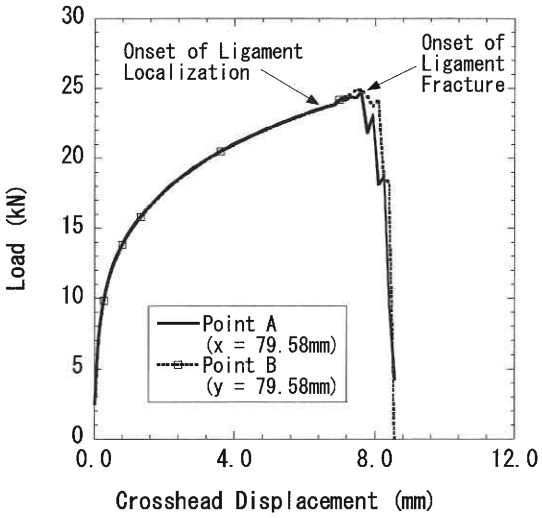

Fig. 10 Load-displacement curve (biaxial loading)

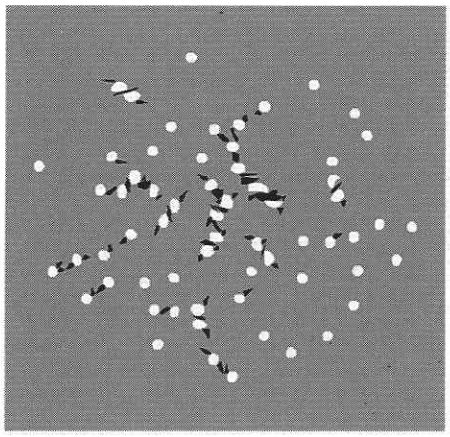

Fig.11 Void linking (biaxial loading, $\delta_x = \delta_y = 7.615$ mm)

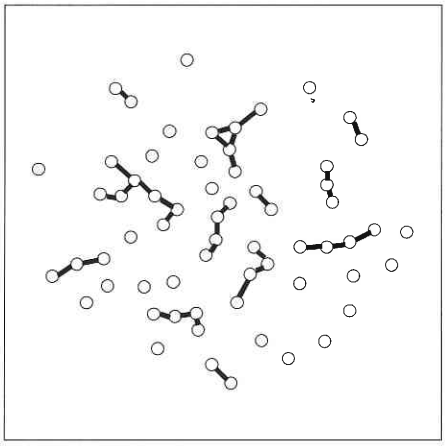

Fig. 12 Experimental void linking (biaxial loading)

4. Concluding Remarks

The mesoscopic method of analysis proposed by the authors has been applied to the elasto-plastic fracture analysis considering void linking. The calculated results for the void linking under uniaxial as well as biaxial loading have agreed well with the experimental results given by Geltmacher *et al.*

(Manuscript received, August 5, 2003)

References

1) Sukumar, N., Moran, B. and Belytschko, T., Int. J. Numer. Meth. Engng., 43, (1998), 839–887.
2) Toi, Y. and Kang, S.-S., Trans. Japan Soc. Mech. Engineers, 68–668, (2002), 588–594.
3) Toi, Y. and Kang, S.-S., *ibid.*, 68–668, (2002), 595–602.
4) Toi, Y. and Kang, S.-S., *ibid.*, 69–683, (2003), 1101–1107.
5) Toi, Y. and Kang, S.-S., *ibid.*, 69–683, (2003), 1108–1113.
6) Geltmacher, A. B. *et al.*, Acta Mater., 44–6, (1996), 2201–2210.